

Manipulating photonic quantum states with long-range interactions

Fan Yang,¹ Yong-Chun Liu,^{1,2,*} and Li You^{1,2,†}

¹*State Key Laboratory of Low Dimensional Quantum Physics,
Department of Physics, Tsinghua University, Beijing 100084, China*
²*Collaborative Innovation Center of Quantum Matter, Beijing, China*

We present a scheme for coherently manipulating quantum states of photons by incorporating multiple photonic modes in a system with long-range interactions. The presence of nonlocal photon-photon interactions destroys the energy or momentum matching conditions between distinct propagating polaritons, and consequently gives rise to blockaded effective coupling between the corresponding polaritons. Such a blockade mechanism protects the system from interaction-induced dissipations and enables highly tunable few-photon nonlinearities. Taking Rydberg atomic ensemble as an example, we illustrate several intriguing phenomena based on the proposed scheme, e.g., the deterministic generation of entangled photon pairs, the nonlinear beam splitting, as well as the establishment of a tunable dressed interaction between individual photons.

I. INTRODUCTION

Strong interactions between light quanta or photons can provide effective control of their quantum states [1]. Significant progresses have been made towards realizing strong photonic nonlinearities [1–3], which cultivated the development of research fields ranging from quantum information processing [4–6] to simulating many-body physics [7–10]. One feasible realization employs strong coupling between highly localized single photons and a single quantum emitter to generate local Kerr nonlinearity [11–14]. Alternatively, effective long-range interactions can be realized by coupling propagating photons to atomic vapor ensembles [2, 3] or atomic arrays in waveguide QED systems [15, 16].

A widely discussed scheme for strong and nonlocal optical nonlinearity is based on electromagnetically induced transparency (EIT) inside a medium of Rydberg atoms [17–22]. The nonlinearity in this system arises from EIT blockade where a multi-photon input destroys the EIT condition [17], and gives rise to a variety of desirable features [19–24]. Most of the earlier studies involve one type of photonic mode, inevitably limiting the scopes and capabilities of photonic information processing. In addition, unavoidable dissipation associated with EIT blockade can cause spatial decoherence to the lone photonic mode, which erects a performance bottleneck for several key applications [25, 26].

We show in this work that by incorporating additional photonic modes and long-range photon-photon interactions, flexible and coherent manipulation of photonic quantum states can be carried out with high fidelities. In contrast to the pioneering proposal of Ref. [27] based on interaction caused polariton mode conversion, our scheme makes use of mode conversion blockade from interaction caused mismatches. Photonic polaritons satisfying energy and momentum matching conditions can ef-

fectively couple to one another during propagation [28]. The presence of strong and long-range photonic interactions destroys the matching conditions, and consequently causes multi-excitations of the nonlinear modes to be blockaded. The subsequent evolution thus restricts the system to an interaction-free subspace, immune to interaction-induced dissipations. Such a blockade mechanism enables the flexible control of few-photon nonlinearities, and facilitates a variety of quantum information protocols, as discussed below.

II. A GENERIC MODEL

In this section, we build up a generic model to describe the basic blockade mechanism, which is not restricted to specific realizations. To illustrate our idea, we first consider two counterpropagating photons, Appendix A details the case for copropagating. Four photonic polariton fields are involved, of which the two forward (backward) propagating ones are described by their slowly-varying operators $\hat{\Psi}_{a_+}(z)$ and $\hat{\Psi}_{b_+}(z)$ [$\hat{\Psi}_{a_-}(z)$ and $\hat{\Psi}_{b_-}(z)$], with μ_{\pm} ($\mu = a, b$) denoting specific polariton modes. Modes a_{\pm} and b_{\pm} are linearly coupled. Photons in modes a_+ and a_- interact nonlocally, while photons in all other modes are assumed noninteracting. The Hamiltonian of our model takes the form $\hat{H} = \hat{H}_0^+ + \hat{H}_0^- + \hat{H}_c^+ + \hat{H}_c^- + \hat{H}_{\text{int}}$, where

$$\hat{H}_0^{\pm} = - \sum_{\mu=a,b} \pm i v_{\pm} \int dz \hat{\Psi}_{\mu}^{\dagger}(z) \partial_z \hat{\Psi}_{\mu}(z), \quad (1)$$

$$\hat{H}_c^{\pm} = \int dz g_{\pm} \hat{\Psi}_{a_{\pm}}^{\dagger}(z) \hat{\Psi}_{b_{\pm}}(z) e^{i \Delta k_{\pm} z} + \text{H.c.}, \quad (2)$$

$$\hat{H}_{\text{int}} = \int dz dz' \mathcal{V}(r) \hat{\Psi}_{a_+}^{\dagger}(z) \hat{\Psi}_{a_-}^{\dagger}(z') \hat{\Psi}_{a_-}(z') \hat{\Psi}_{a_+}(z), \quad (3)$$

denote the equivalent photon kinetic energy with group velocity v_{\pm} , the beam-splitting coupling with strength g_{\pm} and detuning Δk_{\pm} , and the nonlocal two-body interaction via potential $\mathcal{V}(r)$ with $r = z - z'$, respectively.

The evolution of the two-photon quantum state $|\psi(t)\rangle$ is described by the two-photon wavefunction

* yliu@mail.tsinghua.edu.cn

† lyou@mail.tsinghua.edu.cn

$\Psi_{\mu_+\nu_-}(z_1, z_2, t) = \langle 0 | \hat{\Psi}_{\mu_+}(z_1) \hat{\Psi}_{\nu_-}(z_2) | \psi(t) \rangle$. Defining center-of-mass and relative coordinates $R = (v_-z_1 + v_+z_2)/(v_+ + v_-)$ and $\rho = z_1 - (v_-/v_+)z_2$, and moving into the retarded time frame with $\tau = t - \rho/v_{\text{eff}}$, $\xi = t$, and $v_{\text{eff}} = (v_+^2 + v_-^2)/v_+$, one obtains $i\partial_\xi\psi = \mathcal{H}\psi$, where

$$\psi = \left(\tilde{\Psi}_{a_+a_-}, \tilde{\Psi}_{a_+b_-}, \tilde{\Psi}_{b_+a_-}, \tilde{\Psi}_{b_+b_-} \right)^T \quad (4)$$

is the two-photon wavefunction in the rotating frame, and the effective Hamiltonian becomes

$$\mathcal{H} = \begin{pmatrix} v_+\Delta k_+ - v_-\Delta k_- + \mathcal{V} & g_- & g_+ & 0 \\ g_- & v_+\Delta k_+ & 0 & g_+ \\ g_+ & 0 & -v_-\Delta k_- & g_- \\ 0 & g_+ & g_- & 0 \end{pmatrix}. \quad (5)$$

The potential $\mathcal{V}(r)$ is in general a function of both τ and ξ . However, if the long-range interaction is strong enough to meet the condition $|\mathcal{V}| \gg g_\pm, v_\pm |\Delta k_\pm|$ for all r within the range of the wavefunction, the conversion of $\tilde{\Psi}_{a_+b_-}$ and $\tilde{\Psi}_{b_+a_-}$ to $\tilde{\Psi}_{a_+a_-}$ will both be blocked due to the large energy detuning (or momentum mismatch), irrespective of the exact value or form of \mathcal{V} . This coupling blockade for propagating photons arises with long-range interaction, which forbids multi-excitations of the nonlocal nonlinear mode, with its desirable features reminiscent of the widely discussed Rydberg blockade [29–31].

III. BLOCKADE MECHANISM IN RYDBERG EIT SYSTEMS

Various approaches for realizing strong nonlocal interaction between individual photons are discussed [15–17]. In this study, we adopt the Rydberg EIT implementation [17] with mode a_\pm the dark state polariton (DSP) $\hat{\Psi}_{a_\pm}(z) = \cos\theta\hat{\mathcal{E}}_{a_\pm}(z) - \sin\theta\hat{\mathcal{S}}_{a_\pm}(z)$, a superposition of electromagnetic field $\hat{\mathcal{E}}_{a_\pm}(z)$ and Rydberg spin-wave field $\hat{\mathcal{S}}_{a_\pm}(z)$, with $\tan\theta = g_p/\Omega$, g_p the collective atom-photon coupling strength, and Ω the Rabi frequency of the control field [32]. The van der Waals interaction $V(r) = C_6/r^6$ between the Rydberg spin-wave components $\hat{\mathcal{S}}_{a_\pm}(z)$ can induce strong and long-range interactions between DSP modes a_+ and a_- [2].

We present two practical implementations for constructing the linear coupling Hamiltonian. (i) In the photonic coupling scheme shown in Figs. 1(a) and 1(b), we take $\hat{\Psi}_{b_\pm}(z) = \hat{\mathcal{E}}_{b_\pm}(z)$ to be an electromagnetic field of a linear slow-light mode and $\hat{\Psi}_{a_\pm}(z)$ to be a nonlinear DSP that for example can be produced in a hollow-core waveguide filled with Rydberg atoms [33–37]. The beam-splitting coupling $g_\pm \sec\theta\hat{\mathcal{E}}_{a_\pm}^\dagger(z)\hat{\mathcal{E}}_{b_\pm}(z) + \text{H.c.}$ can be obtained from overlapping their evanescent fields. (ii) For the atomic coupling scheme shown in Figs. 1(c) and 1(d), $\hat{\Psi}_{b_\pm}(z)$ represents a linear DSP composed of σ_+ photonic field $\hat{\mathcal{E}}_{\odot_\pm}(z)$ and ground state spin wave field $\hat{\mathcal{S}}_{b_\pm}(z)$, and

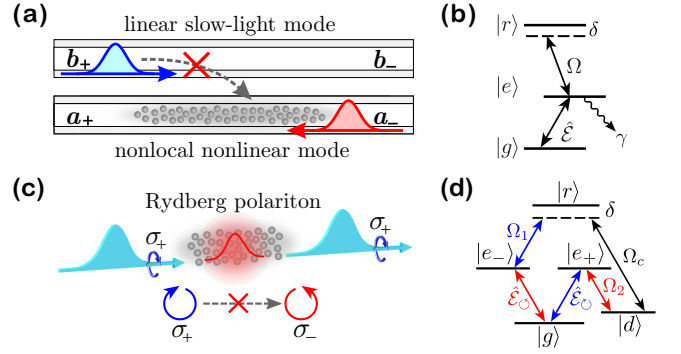


FIG. 1. (a) A schematic for the coupling blockade for counter-propagating photons in a waveguide-like system. (b) Rydberg EIT level diagram, in which the ground state $|g\rangle$, the excited state $|e\rangle$ (linewidth 2γ), and the Rydberg state $|r\rangle$ are coupled respectively by a quantum probe field $\hat{\mathcal{E}}$ and a classical control field Ω , with a two-photon detuning δ . (c) Spin-flip blockade of the propagating photons and (d) the associated atomic level structure.

$\hat{\Psi}_{a_\pm}(z)$ denotes a nonlinear DSP as a superposition of σ_- photonic field $\hat{\mathcal{E}}_{\odot_\pm}(z)$ and Rydberg spin wave $\hat{\mathcal{S}}_{a_\pm}(z)$. The linear coupling $g_\pm \csc^2\theta\hat{\mathcal{S}}_{a_\pm}^\dagger(z)\hat{\mathcal{S}}_{b_\pm}(z) + \text{H.c.}$ can be controlled by the external field Ω_c . In the slow-light regime, influences of coupling to bright state polaritons (BSPs) in the above two schemes are negligible. For simplicity, we assume that mode a_\pm and b_\pm propagate with matched group velocities, while a small mismatch does not significantly influence the coupling between them for short operation time (see Appendix D).

In the conventional EIT blockade [17], a dispersive photonic interaction can be established by using a large single-photon detuning Δ , which, however, results in a large group velocity dispersion and can limit the performance of related applications [38]. For this reason, we take $\Delta = 0$ in this work, where the induced interaction between nonlinear DSPs is highly dissipative. With the proposed blockade mechanism, we can transform such a dissipative interaction into a dispersive one, and achieve coherent manipulations of photonic quantum state.

To clarify the blockade mechanism, we take the backward photon to be a stored gate photon ($g_-, v_- = 0$). In the Rydberg EIT implementation, this can be achieved by taking $\hat{\Psi}_{a_-}(z) = \hat{\mathcal{S}}_-(z)$ to be a stored spin wave of an auxiliary Rydberg state. The parameters for the forward target photon are $g_+ = g$, $v_+ = v$, and $\Delta k_+ = 0$.

For photonic coupling scheme, the spatial modulation of g is considered, i.e., $g = g(z)$. The corresponding dynamics can be described by the two-photon wavefunction $E_a S = \langle 0 | \hat{\mathcal{E}}_{a_+}(z_1) \hat{\mathcal{S}}_-(z_2) | \psi(t) \rangle$ and $E_b S = \langle 0 | \hat{\mathcal{E}}_{b_+}(z_1) \hat{\mathcal{S}}_-(z_2) | \psi(t) \rangle$, which in the frequency domain, to the lowest order of frequency ω , are governed by

$$-i\partial_{z_1} \begin{pmatrix} E_a S \\ E_b S \end{pmatrix} = \begin{pmatrix} \mathcal{V}_0 + \omega(1 + \mathcal{V}_1)/v & g \sec\theta/c \\ g \sec\theta/v & \omega/v \end{pmatrix} \begin{pmatrix} E_a S \\ E_b S \end{pmatrix}, \quad (6)$$

with $\mathcal{V}_0 = ig_p^2/\gamma c(1 - i\Omega^2/\gamma V)$, $\mathcal{V}_1 = g_p^2V[(1 + \gamma^2/\Omega^2)V - 2i\gamma]\cos^2\theta/(\Omega^2 + i\gamma V)^2$, and $v = c\cos^2\theta$. In the absence of interaction ($V = 0$), the coupling between E_aS and E_bS is momentum-matched. With the interaction $V \neq 0$, the strong dissipative interaction $\mathcal{V}_0 \approx ig_p^2/\gamma c$ inside the EIT blockade radius z_b [$V(z_b) = \Omega^2/\gamma$] destroys this matching condition, and the conversion of E_bS to E_aS is blocked if $g_p^2/\gamma c \gg g/v$. As a result of the blockade, the state evolution is restricted to the interaction-free subspace E_bS , endowed with a small decay coefficient $g^2\gamma c/g_p^2v^2$ and a slightly modified group velocity $v/[1 + g^2(\Omega^2 + \gamma^2)/(g_p^2\Omega^2\cos^2\theta)]$. Thus, the strong interaction-induced dissipations are suppressed.

For atomic coupling scheme, the temporal modulation $g = g(t)$ is chosen. In this case, we introduce two-photon wavefunctions $\Psi_\mu S$, $\Phi_\mu S$, $P_\mu S$ to describe DSP, BSP, and the excited state field of mode μ_+ ($\mu = a, b$). Given a V , the dynamics can be described in the momentum-space (transforming from z_1 to k). Up to the first order of k , the equations of motion are approximately given by

$$i\partial_t \begin{pmatrix} \hat{\psi} \\ \Psi_b S \end{pmatrix} = \begin{pmatrix} \hat{V}(k) + k\hat{v} & \hat{g} \\ \hat{g}^\dagger & kc\cos^2\theta \end{pmatrix} \begin{pmatrix} \hat{\psi} \\ \Psi_b S \end{pmatrix}, \quad (7)$$

where $\hat{\psi} = (\Psi_a S, \Phi_a S, P_a S)^T$, $\hat{g} = (g, -g\cot\theta, 0)^T$, $\hat{v} = \text{diag}(c\cos^2\theta, c\sin^2\theta, 0)$, and the effective potential $\hat{V}(k)$ is a matrix of k (see Appendix B). For the noninteracting case, Eq. (7) describes an energy resonant coupling between $\Psi_b S$ and $\Psi_a S$. With a strong interaction V , the dynamics of $\hat{\psi}$ governed by $\hat{V}(k)$ carry dissipative component. However, if the energy detuning induced by $\hat{V}(k)$ ($\sim V\sin^2\theta$) is much stronger than the coupling induced by \hat{g} ($\sim g$), the coupling between $\Psi_b S$ and the interacting space $\hat{\psi}$ can be successfully blocked, with the range characterized by the coupling blockade radius r_b defined as $V(r_b)\sin^2\theta = 2g$ (to be distinguished from z_b). Inside r_b , the dynamics can be described in the $\Psi_b S$ space with hardly modified eigen energy and group velocity, where interaction-induced dissipations are largely suppressed.

For spatial and temporal modulation of the coupling considered above, blockade originates respectively from the interaction caused momentum-mismatch and energy off-resonance. We will focus on temporal modulation with atomic coupling scheme in this study, since it supports richer applications (see Appendix C). In this case, the coupling g is turned on when two photons are close to each other, and is turned off before they completely separate. Thus, for photons with compressed pulse length σ , an ideal blockade requires $\sigma + \frac{1}{2}(v_+ + v_-)t < r_b$ (which reduces to $\sigma < r_b$ for copropagating photons), as otherwise photons separated by more than r_b apart do not feel the blockade. Since EIT displays a finite transparency window, a smaller σ will cause a proportionally larger linear loss. This leads to a tradeoff between ideal blockade and linear loss, which can be relaxed by increasing the blockade optical depth $d_b = g_p^2 z_b/\gamma c$ of the system (see Appendix D).

Although we focus on Rydberg EIT system, the extension to other photonic systems with long-range interactions is straightforward, e.g., waveguide QED systems [15, 16]. In fact, the specific forms of interactions depend on implementations, but the generic form of Eq. (3) applies, as long as the coupling between the interaction-free subspace and Ψ_{a_+, a_-} is blocked (because the interacting detail of Ψ_{a_+, a_-} becomes unimportant in this case). Thus, we will use the generic model to illustrate the basic physics in the next section, while in numerical simulations we consider the full dynamics governed by complete Rydberg EIT coupled equations (see Appendix B).

The calculations are based on solving a set of coupled one-dimensional partial differential equations for two-particle wavefunctions. In the simulation, we assume a uniform atomic density and a square pulse of the coupling field $\Omega_c(t)$ for simplicity. We also neglect the spontaneous decay or dephasing of the Rydberg spin-wave field, since the propagation time inside the atomic ensemble is small enough (see Appendix D).

IV. APPLICATIONS

A. Single-photon quantum switch

As in the previous section, if we take the backward photon to be a stored gate excitation, the equation of motion described by the generic model now reduces to

$$i\partial_\xi \begin{pmatrix} \Psi_{a_+ a_-} \\ \Psi_{b_+ a_-} \end{pmatrix} = \begin{pmatrix} \mathcal{V}(r) & g \\ g & 0 \end{pmatrix} \begin{pmatrix} \Psi_{a_+ a_-} \\ \Psi_{b_+ a_-} \end{pmatrix}. \quad (8)$$

In the absence of \mathcal{V} , the forward photon undergoes complete Rabi oscillation between mode a_+ and b_+ . As explained previously, if $|\mathcal{V}(r)| \gg g$ is satisfied for all r within the spread range of the photon, the coupling between b_+ and a_+ becomes blocked everywhere. Such a phenomenon can be used to implement a single-photon optical switch. For a coupling duration $t = \pi/2g$, the target photon in mode b_+ is transformed to mode a_+ in the absence of the gate photon. This mode conversion becomes blocked if the gate photon is present. As shown in Fig. 2(a), the switching fidelity becomes higher when the blockade radius r_b is sufficiently longer compared with σ . Figure 2(b) displays a typical calculated switching function for $r_b/\sigma = 3$. At $t = \pi/g$, the system functions as a π -phase gate, which gives $\Psi_{b_+ a_-}(z_1, z_2, t) = e^{i\pi}\Psi_{b_+ a_-}(z_1 - vt, z_2, 0)$ for $\mathcal{V} = 0$, and $\Psi_{b_+ a_-}(z_1, z_2, t) = \Psi_{b_+ a_-}(z_1 - vt, z_2, 0)$ for $|\mathcal{V}(\sigma)| \gg g$.

B. Entangled state generation

To generate entanglement between two photonic modes, we take a_- and b_- to be backward propagating modes of a_+ and b_+ with $v_\pm = v$, $\pm\Delta k_\pm = \Delta k$, and $g_\pm = g$. Introducing the symmetric wavefunction

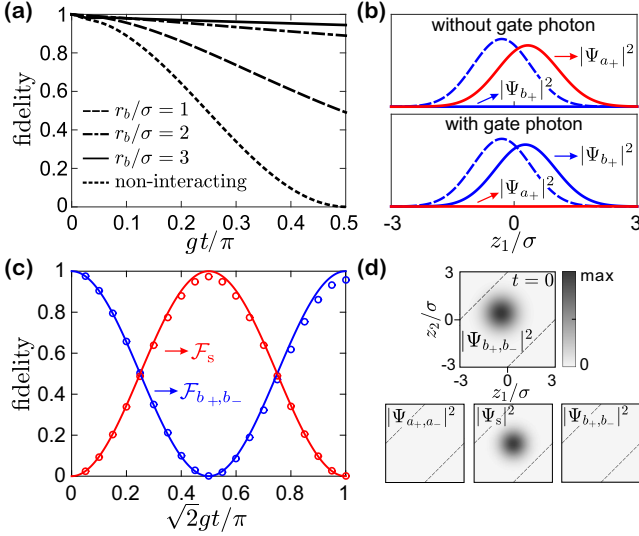


FIG. 2. (a) Evolution of the switching fidelity for different pulse lengths. (b) Evolution of the target photon wavefunction in mode a_+ ($|\Psi_{a_+}(z_1)|^2$) and b_+ ($|\Psi_{b_+}(z_1)|^2$) with $\sigma = r_b/3$ and $gt = \pi/2$, where the dashed line represents the initial wavefunction in mode b_+ . (c) Evolution of fidelities \mathcal{F}_s and \mathcal{F}_{b_+,b_-} . The circles denote numerical calculations and the solid lines represent expected sinusoidal oscillation. (d) Two-photon wavefunctions of the entangled state produced ($\mathcal{F}_s = 97.26\%$) at $\sqrt{2}gt = \pi/2$ with $\sigma = r_b/3$. The simulation is carried out for $\Omega/2\pi = 5$ MHz, $g_p/2\pi = 20$ GHz, $\gamma/2\pi = 3$ MHz, $z_b = 13.8\mu\text{m}$, and $r_b = 16.5\mu\text{m}$. The results are insensitive to the choices of parameters over a broad range. We consider a small group velocity mismatch in (a) and (b) by taking $\Omega_2 = \Omega = 0.9\Omega_1$, and neglect the linear loss of mode b_{\pm} in (c) and (d) (see Appendix B).

$\tilde{\Psi}_s = (\tilde{\Psi}_{a_+b_-} + \tilde{\Psi}_{b_+a_-})/\sqrt{2}$, the Hamiltonian for the generic model reduces to

$$\mathcal{H} = \begin{pmatrix} 2v\Delta k + \mathcal{V}(r) & \sqrt{2}g & 0 \\ \sqrt{2}g & v\Delta k & \sqrt{2}g \\ 0 & \sqrt{2}g & 0 \end{pmatrix}, \quad (9)$$

and the state is given by $\psi = (\tilde{\Psi}_{a_+a_-}, \tilde{\Psi}_s, \tilde{\Psi}_{b_+b_-})^T$. As explained previously, strong interaction can block the excitation of Ψ_{a_+,a_-} , so that photons initially residing in state $|b_+, b_-\rangle$ can be efficiently transferred to an entangled state $|\Psi_s\rangle = (|a_+, b_-\rangle + |b_+, a_-\rangle)/\sqrt{2}$. For the initial state $\tilde{\Psi}_{b_+,b_-}(R, r, t=0) = \Psi_0(R, r)$, the state evolution is given by $\tilde{\Psi}_s(R, r, t) = -i\Psi_0(R, r - 2vt)\sin(\sqrt{2}gt)$, and $\tilde{\Psi}_{b_+,b_-}(R, r, t) = \Psi_0(R, r - 2vt)\cos(\sqrt{2}gt)$, which corresponds to a Rabi oscillation between the initial and the entangled state at an enhanced rate $\sqrt{2}g$, in agreement with numerical results shown in Fig. 2(c). Thus, starting with a separable state $|b_+, b_-\rangle$, an entangled photon pair appears with a high fidelity at $t = \pi/2\sqrt{2}g$ [see Fig. 2(d)].

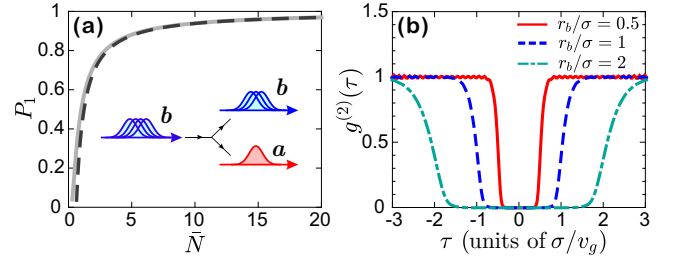


FIG. 3. (a) Single photon output efficiency as a function of the mean photon number \bar{N} for a coherent state input. The solid and dashed lines represent the numerical summation results and the asymptotic solution $1 - \pi^2/(16\bar{N})$, respectively. (b) Second order correlation functions of the output state for a weak coherent input at different values of pulse length σ . The parameters are the same as in Fig. 2(c).

C. Nonlinear beam splitting

The input photonic state $(1/\sqrt{n!}) \left[\int dz h(z) \hat{\Psi}_b^\dagger(z) \right]^n |0\rangle$ containing no photon in mode a and n copropagating photons in mode b with identical wavefunction $h(z)$ is denoted by $|0, n\rangle$. The classical linear beam splitting coupling transforms $\hat{\Psi}_b(z)$ into $T\hat{\Psi}_b(z) + R\hat{\Psi}_a(z)$, whose output state $|\psi(t)\rangle = \sum_m \sqrt{n!/m!(n-m)!} T^{n-m} R^m |m, n-m\rangle$ inevitably includes multi-excitations of mode a .

When a sufficiently strong $|\mathcal{V}(r)| \gg g\sqrt{n}$ is present for all $|r| \lesssim \sigma$, multi-excitations are blocked, and the initial state $|0, n\rangle$ is only effectively coupled to $|1, n-1\rangle$, giving rise to nonlinear beam splitting [see the inset of Fig. 3(a)]. Tracing out mode b , excitation probabilities for the vacuum $|0_a\rangle\langle 0_a|$ and single-photon state $|1_a\rangle\langle 1_a|$ are found to be $p_{0,n} = \cos^2(\sqrt{n}gt)$ and $p_{1,n} = \sin^2(\sqrt{n}gt)$, respectively. For an arbitrary incoming state with photon number distribution probability f_n , the single photon excitation probability becomes $P_1 = \sum_n f_n p_{1,n}$. For a coherent input of a mean photon number \bar{N} ($f_n = \bar{N}^n e^{-\bar{N}}/n!$) and an operating time $t = \pi/(2\sqrt{N}g)$, we find $P_1 \approx 1 - \pi^2/(16\bar{N})$ when \bar{N} is large [see Fig. 3(a)].

Such a nonlinear beam splitting can yield efficient single photon emission from a classical state. Different from the Rydberg EIT absorption protocol which always reduces the state purity [25], the single-photon quantum state obtained here is pure for ideal blockade. Its second order correlation function $g^{(2)}(\tau)$ for a weak coherent input state at $t = \pi/2g$ is shown in Fig. 3(b). As expected, the resulting anti-bunching region is distinguished by the blockade radius r_b , and a pulse with $\sigma < r_b$ can thus deterministically generate single-photons.

D. Tunable dressed interaction

Although bare interactions remain for photons populating the interacting two-photon mode, off-resonant couplings with the interacting nonlinear mode can further

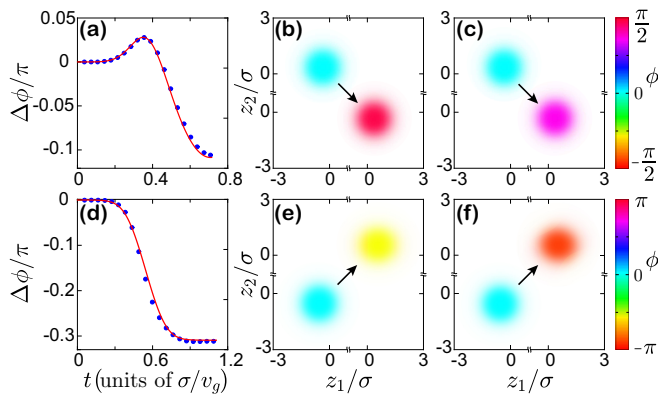


FIG. 4. Dressed interaction induced phase shifts $\Delta\phi = \phi_b - \phi_n$, with ϕ_b and ϕ_n the phase shift for the blockaded and non-interacting case, respectively. (a)-(c) show the counterpropagating case with non-adiabatic manipulations. $\Delta k = 6.25/\sigma$ is used with all other parameters the same as in Fig. 2(c). At $t = 0.71\sigma/v_g$, the fidelity reaches 92.69% and 94.72% for the non-interacting [Fig. 4(b)] and blockaded [Fig. 4(c)] case, respectively. (d)-(f) show the copropagating case with adiabatic manipulations, with $\sigma = 6.51\mu\text{m}$, $\Delta k = 13.20/\sigma$, and $g(t)/v_g\Delta k = [\tanh(5.78v_g t/\sigma - 2.2) - \tanh(5.78v_g t/\sigma - 4.1)]/4$. At $t = 1.09\sigma/v_g$, the fidelity becomes 93.04% and 91.45% for the non-interacting [Fig. 4(e)] and blockaded [Fig. 4(f)] cases, respectively. In (a) and (d), the solid lines and circles respectively denote analytical and numerical results. In (b), (c), (e), and (f), the color and the opacity reflect the phase and the modulus square of the wavefunctions, respectively.

contribute dressed interactions to the noninteracting linear mode, in the same manner as the Rydberg-dressing [39, 40]. One particular advantage is that in the blockade regime ($|\mathcal{V}(r < \sigma)| \gg g, v\Delta k$), these dressed interactions are uniform within the spread range of the photonic wavefunction. Its strength for no photon populating the interacting mode is

$$J_{bb} = -\frac{v\Delta k}{2} + \sqrt{(v\Delta k)^2 + 4g^2} - \frac{1}{2}\sqrt{(v\Delta k)^2 + 8g^2}, \quad (10)$$

and the strength for only one photon populating the interacting mode is

$$J_{ab} = -\frac{v\Delta k}{2} + \frac{1}{2}\sqrt{(v\Delta k)^2 + 8g^2}. \quad (11)$$

In the blockade regime, the dressed interaction strength only depends on tunable parameters Δk and g , which enables the construction of a tunable controlled-phase gate. Figure 4 presents such a plausible implementation with

Rydberg EIT system, where in Figs. 4(a)-4(c), the interaction between two counterpropagating photons initially in the state $|b_+, b_-\rangle$ is considered. Turning on the coupling g when the two photons enter the blockade region and turning it off before they leave, a phase accumulation $\Delta\phi$ can be obtained. For this nonadiabatic manipulation with moderate dressing ($g \lesssim v\Delta k$), a high-fidelity gate requires a suitably controlled operation time. An alternative choice comes from employing copropagating photons with adiabatic manipulations [Figs. 4(d)-4(f)], where the initial state $|a, b\rangle$ is kept in one of the dressed state when g is adiabatically ramped up and down. The wavefunction Ψ_{ab} picks up a dynamic phase $\Delta\phi = -\int dt' J_{ab}(t')$ when g is arranged to change along a closed path with no net flux. Comparisons between the non-interacting calculations [Figs. 4(b) and 4(e)] and the blockaded results [Figs. 4(c) and 4(f)] clearly demonstrate the dressed interaction induced phase shifts.

V. SUMMARY

We show linearly coupled photonic systems with long-range interactions can exhibit coupling blockade for propagating photons. Several rudimentary quantum information protocols facilitated by such a blockade are discussed, including single-photon switching, entangled photon-pair generation, efficient single-photon emission, and photonic phase gate. Our proposal can be realized in photonic waveguide [37] or in atomic vapor [41], and the detailed experimental requirements taking into account the linear EIT loss, imperfect blockade, and group velocity mismatch are discussed in the Appendix D. In addition to photonic quantum state manipulation and their possible extensions to quantum information processing, the mechanism we discuss opens an exciting avenue towards constructing tunable and lossless photon-photon interactions in quantum nonlinear optics.

ACKNOWLEDGMENTS

This work is supported by the National Key R&D Program of China (Grant No. 2018YFA0306503 and No. 2018YFA0306504) and by NSFC (Grant No. 11574177, No. 91636213, No. 11654001, No. 11674390, and No. 91736106). Fan Yang acknowledges helpful discussions with Chuyang Shen, Cheng Chen, Dr. Shen Dong, and Dr. Lin Li.

Appendix A: Equations of motion for counterpropagating and copropagating photons

In this section, we provide a detailed derivation of the Schrodinger-like equations for describing the evolution of the two-photon wavefunctions in the generic model.

In the case of two counterpropagating photons, the model Hamiltonian is described by Eqs. (1)-(3). With the

commutation relation $[\Psi_\mu(z, t), \Psi_\nu^\dagger(z', t)] = \delta_{\mu\nu}\delta(z - z')$ for bosonic particles, the Heisenberg equations for the field operators are given by

$$\partial_t \hat{\Psi}_{a_+}(z) = -v_+ \partial_z \hat{\Psi}_{a_+}(z) - ig_+ \hat{\Psi}_{b_+}(z) e^{i\Delta k_+ z} - i \int dz' \mathcal{V}(z - z') \hat{\Psi}_{a_-}^\dagger(z') \hat{\Psi}_{a_-}(z') \hat{\Psi}_{a_+}(z), \quad (\text{A1})$$

$$\partial_t \hat{\Psi}_{b_+}(z) = -v_+ \partial_z \hat{\Psi}_{b_+}(z) - ig_+ \hat{\Psi}_{a_+}(z) e^{-i\Delta k_+ z}, \quad (\text{A2})$$

$$\partial_t \hat{\Psi}_{a_-}(z) = v_- \partial_z \hat{\Psi}_{a_-}(z) - ig_- \hat{\Psi}_{b_-}(z) e^{i\Delta k_- z} - i \int dz' \mathcal{V}(z' - z) \hat{\Psi}_{a_+}^\dagger(z') \hat{\Psi}_{a_+}(z') \hat{\Psi}_{a_-}(z), \quad (\text{A3})$$

$$\partial_t \hat{\Psi}_{b_-}(z) = v_- \partial_z \hat{\Psi}_{b_-}(z) - ig_- \hat{\Psi}_{a_-}(z) e^{-i\Delta k_- z}, \quad (\text{A4})$$

In the Schrodinger picture, the state of the system can be written as

$$|\psi(t)\rangle = \iint dz_1 dz_2 \Psi_{a_+ a_-}(z_1, z_2, t) \hat{\Psi}_{a_+}^\dagger(z_1) \hat{\Psi}_{a_-}^\dagger(z_2) |0\rangle + \iint dz_1 dz_2 \Psi_{a_+ b_-}(z_1, z_2, t) \hat{\Psi}_{a_+}^\dagger(z_1) \hat{\Psi}_{b_-}^\dagger(z_2) |0\rangle \\ + \iint dz_1 dz_2 \Psi_{b_+ a_-}(z_1, z_2, t) \hat{\Psi}_{b_+}^\dagger(z_1) \hat{\Psi}_{a_-}^\dagger(z_2) |0\rangle + \iint dz_1 dz_2 \Psi_{b_+ b_-}(z_1, z_2, t) \hat{\Psi}_{b_+}^\dagger(z_1) \hat{\Psi}_{b_-}^\dagger(z_2) |0\rangle, \quad (\text{A5})$$

where $\Psi_{\mu+\nu-}(z_1, z_2, t) = \langle 0 | \hat{\Psi}_{\mu+}(z_1) \hat{\Psi}_{\nu-}(z_2) | \psi(t) \rangle$ denotes a two-photon wavefunction. With the Heisenberg equations (A1)-(A4), the equation of motion for the two-photon wavefunctions becomes

$$\partial_t \Psi_{a_+ a_-} = -v_+ \partial_{z_1} \Psi_{a_+ a_-} - ig_+ \Psi_{b_+ a_-} e^{i\Delta k_+ z_1} + v_- \partial_{z_2} \Psi_{a_+ a_-} - ig_- \Psi_{a_+ b_-} e^{i\Delta k_- z_2} - i\mathcal{V}(z_1 - z_2) \Psi_{a_+ a_-}, \quad (\text{A6})$$

$$\partial_t \Psi_{a_+ b_-} = -v_+ \partial_{z_1} \Psi_{a_+ b_-} - ig_+ \Psi_{b_+ b_-} e^{i\Delta k_+ z_1} + v_- \partial_{z_2} \Psi_{a_+ b_-} - ig_- \Psi_{a_+ a_-} e^{-i\Delta k_- z_2}, \quad (\text{A7})$$

$$\partial_t \Psi_{b_+ a_-} = -v_+ \partial_{z_1} \Psi_{b_+ a_-} - ig_+ \Psi_{a_+ a_-} e^{-i\Delta k_+ z_1} + v_- \partial_{z_2} \Psi_{b_+ a_-} - ig_- \Psi_{b_+ b_-} e^{i\Delta k_- z_2}, \quad (\text{A8})$$

$$\partial_t \Psi_{b_+ b_-} = -v_+ \partial_{z_1} \Psi_{b_+ b_-} - ig_+ \Psi_{a_+ b_-} e^{-i\Delta k_+ z_1} + v_- \partial_{z_2} \Psi_{b_+ b_-} - ig_- \Psi_{b_+ a_-} e^{-i\Delta k_- z_2}. \quad (\text{A9})$$

Transforming the wavefunctions into the rotating frame, according to

$$\Psi_{a_+, a_-} = \tilde{\Psi}_{a_+, a_-} e^{i(\Delta k_+ z_1 + \Delta k_- z_2)}, \Psi_{a_+, b_-} = \tilde{\Psi}_{a_+, b_-} e^{i\Delta k_+ z_1}, \Psi_{b_+, a_-} = \tilde{\Psi}_{b_+, a_-} e^{i\Delta k_- z_2}, \Psi_{b_+, b_-} = \tilde{\Psi}_{b_+, b_-}, \quad (\text{A10})$$

Eqs. (A6)-(A9) are simplified to

$$(\partial_t + v_+ \partial_{z_1} - v_- \partial_{z_2}) \begin{pmatrix} \tilde{\Psi}_{a_+ a_-} \\ \tilde{\Psi}_{a_+ b_-} \\ \tilde{\Psi}_{b_+ a_-} \\ \tilde{\Psi}_{b_+ b_-} \end{pmatrix} = -i \begin{pmatrix} v_+ \Delta k_+ - v_- \Delta k_- + \mathcal{V}(z_1 - z_2) & g_- & g_+ & 0 \\ g_- & v_+ \Delta k_+ & 0 & g_+ \\ g_+ & 0 & -v_- \Delta k_- & g_- \\ 0 & g_+ & g_- & 0 \end{pmatrix} \begin{pmatrix} \tilde{\Psi}_{a_+ a_-} \\ \tilde{\Psi}_{a_+ b_-} \\ \tilde{\Psi}_{b_+ a_-} \\ \tilde{\Psi}_{b_+ b_-} \end{pmatrix}. \quad (\text{A11})$$

Further introducing center-of-mass and relative coordinates $R = (v_- z_1 + v_+ z_2)/(v_+ + v_-)$ and $\rho = z_1 - (v_-/v_+)z_2$, and moving into the retarded time frame with $\tau = t - \rho/v_{\text{eff}}$ and $\xi = t$, we can obtain Eq. (5) in the main text.

For the case of two copropagating photons, the Hamiltonian of the system is $\hat{H} = \hat{H}_0 + \hat{H}_c + \hat{H}_{\text{int}}$, where

$$\hat{H}_0 = -iv \int dz \hat{\Psi}_a^\dagger(z) \partial_z \hat{\Psi}_a(z) - iv \int dz \hat{\Psi}_b^\dagger(z) \partial_z \hat{\Psi}_b(z), \quad (\text{A12})$$

$$\hat{H}_c = \int dz g \hat{\Psi}_a^\dagger(z) \hat{\Psi}_b(z) e^{i\Delta k z} + \text{H.c.}, \quad (\text{A13})$$

$$\hat{H}_{\text{int}} = \frac{1}{2} \int dz dz' \mathcal{V}(z - z') \hat{\Psi}_a^\dagger(z) \hat{\Psi}_a^\dagger(z') \hat{\Psi}_a(z') \hat{\Psi}_a(z). \quad (\text{A14})$$

The state of the system is described by the two-photon wavefunction $\Psi_{\mu\nu}(z_1, z_2, t) = \langle 0 | \hat{\Psi}_\mu(z_1) \hat{\Psi}_\nu(z_2) | \psi(t) \rangle$, i.e.,

$$|\psi(t)\rangle = \frac{1}{2} \iint dz_1 dz_2 \Psi_{aa}(z_1, z_2, t) \hat{\Psi}_a^\dagger(z_1) \hat{\Psi}_a^\dagger(z_2) |0\rangle + \frac{1}{2} \iint dz_1 dz_2 \Psi_{bb}(z_1, z_2, t) \hat{\Psi}_b^\dagger(z_1) \hat{\Psi}_b^\dagger(z_2) |0\rangle \\ + \iint dz_1 dz_2 \Psi_{ab}(z_1, z_2, t) \hat{\Psi}_a^\dagger(z_1) \hat{\Psi}_b^\dagger(z_2) |0\rangle. \quad (\text{A15})$$

Employing the same procedure as developed for the counterpropagating case, the equations of motion in the moving and rotating frame can be simplified to

$$(\partial_t + v \partial_R) \begin{pmatrix} \tilde{\Psi}_{aa} \\ \tilde{\Psi}_{ab} \\ \tilde{\Psi}_{ba} \\ \tilde{\Psi}_{bb} \end{pmatrix} = -i \begin{pmatrix} 2v\Delta k + \mathcal{V}(r) & g & g & 0 \\ g & v\Delta k & 0 & g \\ g & 0 & v\Delta k & g \\ 0 & g & g & 0 \end{pmatrix} \begin{pmatrix} \tilde{\Psi}_{aa} \\ \tilde{\Psi}_{ab} \\ \tilde{\Psi}_{ba} \\ \tilde{\Psi}_{bb} \end{pmatrix}. \quad (\text{A16})$$

In the calculations, the fidelity $\mathcal{F}_{\mu\nu}$ and the phase $\phi_{\mu\nu}$ to the state $\hat{U}_0(t, 0) \iint dz_1 dz_2 \Psi_0(z_1, z_2) \hat{\Psi}_{\mu_+}^\dagger(z_1) \hat{\Psi}_{\nu_-}^\dagger(z_2) |0\rangle$ is determined by

$$\sqrt{\mathcal{F}_{\mu\nu}} e^{i\phi_{\mu\nu}} = \int dz_1 dz_2 \Psi_0^*(z_1 - v_+ t, z_2 + v_- t) \Psi_{\mu_+ \nu_-}(z_1, z_2, t), \quad (\text{A17})$$

for two counterpropagating photons (and analogously for two copropagating photons), where $\hat{U}_0(t, 0)$ denotes the noninteracting unitary time-evolution operator, and $\Psi_0(z_1, z_2)$ represents the normalized initial wavefunction (at $t = 0$). The fidelity \mathcal{F}_s for the symmetric entangled state is obtained by replacing the wavefunction $\Psi_{\mu_+ \nu_-}(z_1, z_2, t)$ with $\frac{1}{\sqrt{2}} [\Psi_{a_+ b_-}(z_1, z_2, t) + \Psi_{b_+ a_-}(z_1, z_2, t)]$ in Eq. (A17).

Appendix B: Rydberg EIT implementation

In this section, we describe how to map the Rydberg EIT system to the generic model derived in the previous section. In a Rydberg EIT system [17], the evolution of light and atomic excitations can be described by bosonic operators $\hat{\mathcal{E}}_{a_\pm}^\dagger(z, t)$, $\hat{\mathcal{P}}_{a_\pm}^\dagger(z)$, and $\hat{\mathcal{S}}_{a_\pm}^\dagger(z)$, which create a photon, an atomic spin-wave in intermediate state $|e\rangle$, and an atomic spin-wave in Rydberg state $|r\rangle$, respectively. We take the dark state polariton to be the interacting mode a_\pm , i.e., $\hat{\Psi}_{a_\pm}(z) = \cos\theta \hat{\mathcal{E}}_{a_\pm}(z) - \sin\theta \hat{\mathcal{S}}_{a_\pm}(z)$ with $\tan\theta = g_p/\Omega$ (see the main text).

To gain the essential physics of the coupling blockade, we first consider the simple case with the target photon stored in an auxiliary Rydberg state, i.e., we take $\hat{\Psi}_{a_-}(z) = \hat{\mathcal{S}}_-(z)$. For the photonic coupling scheme, the coupling between a_+ and another linear mode b_+ is obtained through photonic coupling term $g \sec\theta \hat{\mathcal{E}}_{a_+}^\dagger(z) \hat{\mathcal{E}}_{b_+}(z) + \text{H.c.}$, and the equations of motion for the field operators are given by

$$\partial_t \hat{\mathcal{E}}_{a_+}(z) = -c \partial_z \hat{\mathcal{E}}_{a_+}(z) + i g_p \hat{\mathcal{P}}_{a_+}(z) - i g \sec\theta \hat{\mathcal{E}}_{b_+}(z), \quad (\text{B1})$$

$$\partial_t \hat{\mathcal{P}}_{a_+}(z) = -\gamma \hat{\mathcal{P}}_{a_+}(z) + i g_p \hat{\mathcal{E}}_{a_+}(z) + i \Omega \hat{\mathcal{S}}_{a_+}(z), \quad (\text{B2})$$

$$\partial_t \hat{\mathcal{S}}_{a_+}(z) = i \Omega \hat{\mathcal{P}}_{a_+}(z) - i \int dz' V(z - z') \hat{\mathcal{S}}_-^\dagger(z') \hat{\mathcal{S}}_-(z') \hat{\mathcal{S}}_{a_+}(z), \quad (\text{B3})$$

$$\partial_t \hat{\mathcal{E}}_{b_+}(z) = -v \partial_z \hat{\mathcal{E}}_{b_+}(z) - i g \sec\theta \hat{\mathcal{E}}_{a_+}(z), \quad (\text{B4})$$

$$\partial_t \hat{\mathcal{S}}_-(z) = -i \int dz' V(z - z') \hat{\mathcal{S}}_{a_+}^\dagger(z') \hat{\mathcal{S}}_{a_+}(z') \hat{\mathcal{S}}_-(z). \quad (\text{B5})$$

In Eq. (B2), we neglect the Langevin noise terms associated with the decay of the field operator $\hat{\mathcal{P}}_{a_+}(z)$, since they do not affect the calculation of the two-photon wavefunction [17]. Introducing the two-particle wavefunction as in Appendix A, the state $|\psi(t)\rangle$ of the system can be described by $\psi(z_1, z_2, t) = (E_a S, P_a S, S_a S, E_b S)^T$ with each element being a two-particle wavefunction component (e.g., $E_a S = \langle 0 | \hat{\mathcal{E}}_{a_+}(z_1) \hat{\mathcal{S}}_-(z_2) | \psi(t) \rangle$), whose dynamics are governed by

$$\partial_t E_a S(z_1, z_2) = -c \partial_{z_1} E_a S(z_1, z_2) + i g_p P_a S(z_1, z_2) - i g \sec\theta E_b S(z_1, z_2), \quad (\text{B6})$$

$$\partial_t P_a S(z_1, z_2) = -\gamma P_a S(z_1, z_2) + i g_p E_a S(z_1, z_2) + i \Omega S_a S(z_1, z_2), \quad (\text{B7})$$

$$\partial_t S_a S(z_1, z_2) = i \Omega P_a S(z_1, z_2) - i V(z_2 - z_1) S_a S(z_1, z_2), \quad (\text{B8})$$

$$\partial_t E_b S(z_1, z_2) = -v \partial_{z_1} E_b S(z_1, z_2) - i g \sec\theta E_a S(z_1, z_2). \quad (\text{B9})$$

In the photonic coupling scheme, the passive modulation of the coupling g is straightforwardly implemented, i.e., $g = g(z)$. Thus, we solve Eqs. (B6)-(B9) in the frequency domain by applying the Fourier transform of time t , i.e., introducing $\psi(z_1, z_2, \omega) = \int dt e^{i\omega t} \psi(z_1, z_2, t)$. Up to the first order of ω , the equations of motion simplify to Eq. (6). In the blockade region with $|\mathcal{V}_0\rangle \gg g/v$, $E_b S$ is only perturbatively coupled with $E_a S$, and the effective dynamics of $E_b S$ is governed by

$$\partial_{z_1} E_b S = -i \frac{g^2}{(v^2 \mathcal{V}_0)} E_b S - \frac{v}{1 + g^2 \mathcal{V}_1 / v^2 \mathcal{V}_0^2} \partial_t E_b S. \quad (\text{B10})$$

Since $\mathcal{V}_0(r) \approx i g_p^2 / \gamma c$ for $r < z_b$ and $\mathcal{V}_0(r) \approx 0$ for $r > z_b$, [with z_b defined by $V(z_b) = \Omega^2 / \gamma$], coupling blockade in this case requires $g_p^2 / \gamma c \gg g/v$, and the blockade range is characterized by the EIT blockade radius z_b .

For the atomic coupling scheme, the dynamics of the system shown in Fig. 1(d) in the main text can be described by the field operators $\hat{\mathcal{E}}_{a_+}^\dagger(z)$, $\hat{\mathcal{P}}_{a_+}^\dagger(z)$, $\hat{\mathcal{S}}_{a_+}^\dagger(z)$, $\hat{\mathcal{E}}_{b_+}^\dagger(z)$, $\hat{\mathcal{P}}_{b_+}^\dagger(z)$, and $\hat{\mathcal{S}}_{b_+}^\dagger(z)$, which create a photon with polarization a ,

an atomic spin-wave in intermediate state $|e_-\rangle$, an atomic spin-wave in Rydberg state $|r\rangle$, a photon with polarization b , an atomic spin-wave in intermediate state $|e_+\rangle$, and an atomic spin-wave in ground state $|d\rangle$. The coupling between the nonlinear DSP $\hat{\Psi}_{a_+}(z) = \cos\theta_1\hat{\mathcal{E}}_{a_+}(z) - \sin\theta_1\hat{\mathcal{S}}_{a_+}(z)$ and the linear DSP $\hat{\Psi}_{b_+}(z) = \cos\theta_2\hat{\mathcal{E}}_{b_+}(z) - \sin\theta_2\hat{\mathcal{S}}_{b_+}(z)$ is obtained through atomic coupling term $g \csc\theta_1 \csc\theta_2 \hat{\mathcal{S}}_{a_+}^\dagger(z)\hat{\mathcal{S}}_{b_+}(z) + \text{H.c.}$ with $\tan\theta_1 = g_p/\Omega_1$ and $\tan\theta_2 = g_p/\Omega_2$ (assuming $|e_+\rangle$ and $|e_-\rangle$ are of the same hyperfine manifold). The dynamics of these operators are governed by

$$\partial_t \hat{\mathcal{E}}_{a_+}(z) = -c\partial_z \hat{\mathcal{E}}_{a_+}(z) + ig_p \hat{\mathcal{P}}_{a_+}(z), \quad (\text{B11})$$

$$\partial_t \hat{\mathcal{P}}_{a_+}(z) = -\gamma \hat{\mathcal{P}}_{a_+}(z) + ig_p \hat{\mathcal{E}}_{a_+}(z) + i\Omega_1 \hat{\mathcal{S}}_{a_+}(z), \quad (\text{B12})$$

$$\partial_t \hat{\mathcal{S}}_{a_+}(z) = i\Omega_1 \hat{\mathcal{P}}_{a_+}(z) - ig \csc\theta_1 \csc\theta_2 \hat{\mathcal{S}}_{b_+}(z, t) - i \int dz' V(z-z') \hat{\mathcal{S}}_-^\dagger(z') \hat{\mathcal{S}}_-(z') \hat{\mathcal{S}}_{a_+}(z), \quad (\text{B13})$$

$$\partial_t \hat{\mathcal{E}}_{b_+}(z) = -c\partial_z \hat{\mathcal{E}}_{b_+}(z) + ig_p \hat{\mathcal{P}}_{b_+}(z), \quad (\text{B14})$$

$$\partial_t \hat{\mathcal{P}}_{b_+}(z) = -\gamma \hat{\mathcal{P}}_{b_+}(z) + ig_p \hat{\mathcal{E}}_{b_+}(z) + i\Omega_2 \hat{\mathcal{S}}_{b_+}(z), \quad (\text{B15})$$

$$\partial_t \hat{\mathcal{S}}_{b_+}(z) = i\Omega_2 \hat{\mathcal{P}}_{b_+} - ig \csc\theta_1 \csc\theta_2 \hat{\mathcal{S}}_{a_+}(z, t), \quad (\text{B16})$$

$$\partial_t \hat{\mathcal{S}}_-(z) = -i \int dz' V(z-z') \hat{\mathcal{S}}_{a_+}^\dagger(z') \hat{\mathcal{S}}_{a_+}(z') \hat{\mathcal{S}}_-(z), \quad (\text{B17})$$

and the corresponding equations of motion for the two-particle wavefunction are given by

$$\partial_t E_a S(z_1, z_2) = -c\partial_{z_1} E_a S(z_1, z_2) + ig_p P_a S(z_1, z_2), \quad (\text{B18})$$

$$\partial_t P_a S(z_1, z_2) = -\gamma P_a S(z_1, z_2) + ig_p E_a S(z_1, z_2) + i\Omega_1 S_a S(z_1, z_2), \quad (\text{B19})$$

$$\partial_t S_a S(z_1, z_2) = i\Omega_1 P_a S(z_1, z_2) - ig \csc\theta_1 \csc\theta_2 S_b S(z_1, z_2) - iV(z_2 - z_1) S_a S(z_1, z_2), \quad (\text{B20})$$

$$\partial_t E_b S(z_1, z_2) = -c\partial_{z_1} E_b S(z_1, z_2) + ig_p P_b S(z_1, z_2), \quad (\text{B21})$$

$$\partial_t P_b S(z_1, z_2) = -\gamma P_b S(z_1, z_2) + ig_p E_b S(z_1, z_2) + i\Omega_2 S_b S(z_1, z_2), \quad (\text{B22})$$

$$\partial_t S_b S(z_1, z_2) = i\Omega_2 P_b S(z_1, z_2) - ig \csc\theta_1 \csc\theta_2 S_a S(z_1, z_2). \quad (\text{B23})$$

In the atomic coupling scheme, the active modulation of the coupling g is available, i.e., $g = g(t)$. Thus, we can solve Eqs. (B18)-(B23) in the momentum space by applying the Fourier transform $\psi(k, z_2, t) = \int dz_1 e^{-ikz_1} \psi(z_1, z_2, t)$. Following Ref. [8], we set V as a constant to see how the blockade works in this case, while in the numerical simulation V is taken to be position-dependent rigorously. Introducing the bright state polaritons (BSPs) $\hat{\Phi}_{a_+}(z) = \sin\theta_1 \hat{\mathcal{E}}_{a_+}(z) + \cos\theta_1 \hat{\mathcal{S}}_{a_+}(z)$ and $\hat{\Phi}_{b_+}(z) = \sin\theta_2 \hat{\mathcal{E}}_{b_+}(z) + \cos\theta_2 \hat{\mathcal{S}}_{b_+}(z)$, the evolution of the two-photon wavefunction $\psi(z_1, z_2, t) = (\Psi_a S, \Phi_a S, P_a S, \Psi_b S, \Phi_b S, P_b S)^T$ in k -space is governed by $i\partial_t \psi = \mathcal{H}\psi$, with \mathcal{H} given by

$$\mathcal{H} = \begin{pmatrix} ck \cos^2 \theta_1 + V \sin^2 \theta_1 & \sin \theta_1 \cos \theta_1 (ck - V) & 0 & g & -g \cot \theta_2 & 0 \\ \sin \theta_1 \cos \theta_1 (ck - V) & ck \sin^2 \theta_1 + V \cos^2 \theta_1 & -\sqrt{g_p^2 + \Omega_1^2} & -g \cot \theta_1 & g \cot \theta_1 \cot \theta_2 & 0 \\ 0 & -\sqrt{g_p^2 + \Omega_1^2} & -i\gamma & 0 & 0 & 0 \\ g & -g \cot \theta_1 & 0 & ck \cos^2 \theta_2 & ck \sin \theta_2 \cos \theta_2 & 0 \\ -g \cot \theta_2 & g \cot \theta_1 \cot \theta_2 & 0 & ck \sin \theta_2 \cos \theta_2 & ck \sin^2 \theta_2 & -\sqrt{g_p^2 + \Omega_2^2} \\ 0 & 0 & 0 & 0 & -\sqrt{g_p^2 + \Omega_2^2} & -i\gamma \end{pmatrix}. \quad (\text{B24})$$

In the above, the small coupling $-g \cot \theta_2$ between $\Psi_a S$ and $(\Phi_b S, P_b S)$ can be neglected in the slow-light regime ($\cos\theta_{1/2} \ll 1$), and $\Psi_b S$ decouples with $(\Phi_b S, P_b S)$ up to the first order of k . Thus, $(\Phi_b S, P_b S)$ can be dropped out of the dynamics if we neglect the linear loss of $\hat{\Psi}_{b_+}(z)$, and the corresponding equations of motion reduce to

$$i\partial_t \begin{pmatrix} \hat{\psi} \\ \Psi_b S \end{pmatrix} = \begin{pmatrix} \hat{\mathcal{V}}(k) + k\hat{v} & \hat{g} \\ \hat{g}^\dagger & kc \cos^2 \theta_2 \end{pmatrix} \begin{pmatrix} \hat{\psi} \\ \Psi_b S \end{pmatrix}, \quad (\text{B25})$$

where $\hat{\psi} = (\Psi_a S, \Phi_a S, P_a S)^T$, $\hat{g} = (g, -g \cot \theta_1, 0)^T$, $\hat{v} = \text{diag}(c \cos^2 \theta_1, c \sin^2 \theta_1, 0)$, and the effective potential $\hat{\mathcal{V}}(k)$ is

$$\hat{\mathcal{V}}(k) = \begin{pmatrix} ck \cos^2 \theta_1 + V \sin^2 \theta_1 & \sin \theta_1 \cos \theta_1 (ck - V) & 0 \\ \sin \theta_1 \cos \theta_1 (ck - V) & ck \sin^2 \theta_1 + V \cos^2 \theta_1 & -\sqrt{g_p^2 + \Omega_1^2} \\ 0 & -\sqrt{g_p^2 + \Omega_1^2} & -i\gamma \end{pmatrix}. \quad (\text{B26})$$

For the noninteracting case ($V = 0$), Ψ_a decouples with $(\Phi_a S, P_a S)$ up to the first order of k , and the coupling

between $\Psi_b S$ and $(\Phi_a S, P_a S)$ is negligible in the slow-

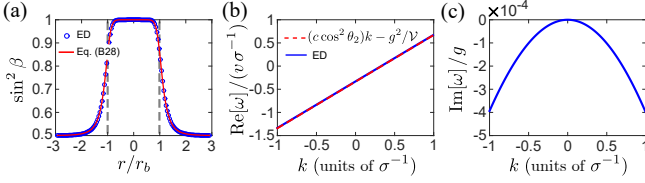


FIG. 5. (a) Weight of the $\Psi_b S$ component in the modified eigen state $\Psi_b S'$ with $k = 0.5/\sigma$. (b) and (c) show the dispersion relation of the modified eigen state $\Psi_b S'$, in which (b) displays the real part of the eigen frequency ω and (c) plots the imaginary part of ω (at $r = 0.8r_b$). The parameters are the same as in Fig. 2 in the main text.

light regime, so that Eq. (B25) can be simplified to

$$i\partial_t \begin{pmatrix} \Psi_a S \\ \Psi_b S \end{pmatrix} = \begin{pmatrix} kc \cos^2 \theta_1 & g \\ g & kc \cos^2 \theta_2 \end{pmatrix} \begin{pmatrix} \Psi_a S \\ \Psi_b S \end{pmatrix}. \quad (\text{B27})$$

For the interacting case ($V \neq 0$), $\hat{V}(k)$ is not diagonal, and the DSP field $\Psi_a S$ is strongly coupled with $\Phi_a S$ and $P_a S$ at $V \approx -g_p^2/(ck)$, which induces strong dissipative dynamics of $\Psi_a S$. In general, the coupling between $\Psi_b S$ and $\hat{\psi}$ can be characterized by the modified eigen state $\Psi_b S'$ through exact diagonalization (ED) of the Hamiltonian in Eq. (B25), which is a linear superposition of $\Psi_b S$ and $\hat{\psi}$, i.e., $\Psi_b S' = \sin \beta \Psi_b S + \cos \beta \hat{w}^\dagger \hat{\psi}$, with \hat{w} being a weight matrix. The ideal blockade requires $\sin \beta \approx 1$, and a smaller $\sin \beta$ indicates a less effective blockade. In the slow-light regime, the eigen energy of $\Psi_a S$ is characterized by $\mathcal{V} = V \sin^2 \theta_1$, and thus the weight can be approximately expressed as

$$\sin^2 \beta \approx 1 - \frac{2(g/\mathcal{V})^2}{1 + (2g/\mathcal{V})^2 + \sqrt{1 + (2g/\mathcal{V})^2}}, \quad (\text{B28})$$

which is verified by rigorous results from ED [see Fig. 5(a)]. With Eq. (B28), we can introduce the coupling blockade radius r_b defined as $\mathcal{V}(r_b) = 2g$, at which we have $\sin \beta \approx 0.9$. Such a blockade radius characterizes the effective blockade range, i.e., the coupling of $\Psi_b S$ to $\hat{\psi}$

can be effectively blocked for $|r| < r_b$ region. Different from spatial modulation, the perturbative coupling with the interacting space induces negligible modifications of $\Psi_b S$ inside the blockade radius r_b . This is verified by the dispersion relation of the modified eigen state $\Psi_b S'$ shown in Figs. 5(b) and 5(c), as the group velocity is rarely changed and the dissipation is negligible during the operation time ($\sim g^{-1}$).

Next, we consider the interaction between two propagating photons. We take counterpropagating photons with atomic coupling scheme as an example, while the generalization to the copropagating case and photonic coupling scheme is straightforward. For simplicity, we drop the field operators $\hat{\Phi}_{b\pm}(z)$ and $\hat{\mathcal{P}}_{b\pm}(z)$ out of the dynamics. As explained previously, this corresponds to neglecting the linear loss of $\hat{\Psi}_{b\pm}(z)$, which is valid as long as the linear loss is small during the operation time. In this case, the equations of motion for the field operators are given by

$$\partial_t \hat{\mathcal{E}}_{a+}(z) = -c\partial_z \hat{\mathcal{E}}_{a+}(z) + ig_p \hat{\mathcal{P}}_{a+}(z), \quad (\text{B29})$$

$$\partial_t \hat{\mathcal{P}}_{a+}(z) = -\gamma \hat{\mathcal{P}}_{a+}(z) + ig \hat{\mathcal{E}}_{a+}(z) + i\Omega \hat{\mathcal{S}}_{a+}(z), \quad (\text{B30})$$

$$\partial_t \hat{\mathcal{S}}_{a+}(z) = i\Omega \hat{\mathcal{P}}_{a+}(z) - ig'_+ \hat{\Psi}_{b+}(z) - i\delta \hat{\mathcal{S}}_{a+}(z) - i \int dz' V(r) \hat{\mathcal{S}}_{a-}^\dagger(z') \hat{\mathcal{S}}_{a-}(z') \hat{\mathcal{S}}_{a+}(z), \quad (\text{B31})$$

$$\partial_t \hat{\Psi}_{b+}(z) = -v\partial_z \hat{\Psi}_{b+}(z) - ig'_+ \hat{\mathcal{S}}_{a+}(z), \quad (\text{B32})$$

$$\partial_t \hat{\mathcal{E}}_{a-}(z) = c\partial_z \hat{\mathcal{E}}_{a-}(z) + ig_p \hat{\mathcal{P}}_{a-}(z), \quad (\text{B33})$$

$$\partial_t \hat{\mathcal{P}}_{a-}(z) = -\gamma \hat{\mathcal{P}}_{a-}(z) + ig \hat{\mathcal{E}}_{a-}(z) + i\Omega \hat{\mathcal{S}}_{a-}(z), \quad (\text{B34})$$

$$\partial_t \hat{\mathcal{S}}_{a-}(z) = i\Omega \hat{\mathcal{P}}_{a-}(z) - ig'_- \hat{\Psi}_{b-}(z) - i\delta \hat{\mathcal{S}}_{a-}(z) - i \int dz' V(r) \hat{\mathcal{S}}_{a+}^\dagger(z') \hat{\mathcal{S}}_{a+}(z') \hat{\mathcal{S}}_{a-}(z), \quad (\text{B35})$$

$$\partial_t \hat{\Psi}_{b-}(z) = v\partial_z \hat{\Psi}_{b-}(z) - ig'_- \hat{\mathcal{S}}_{a-}(z), \quad (\text{B36})$$

where $g'_\pm = g_\pm \csc \theta_1$, δ is the two-photon detuning ($\Delta k_\pm = \delta/v$), and $v = c \cos^2 \theta$ represents the group velocity of the linear DSP field. Introducing the two-particle wavefunction, the state $|\psi(t)\rangle$ of the system can be described by

$$\psi(z_1, z_2, t) = (EE, EP, ES, EB, PE, PP, PS, PB, SA, SP, SS, SB, BE, BP, BS, BB)^T, \quad (\text{B37})$$

with each element being a two-particle wavefunction component (e.g., $BS = \langle 0 | \hat{\Psi}_{b+}(z_1) \hat{\mathcal{S}}_{a-}(z_2) | \psi(t) \rangle$). The equation of motion is determined by $i\partial_t \psi(z_1, z_2, t) = \mathcal{H}(z_1, z_2, t) \psi(z_1, z_2, t)$, where the effective Hamiltonian \mathcal{H} is given by

$$\mathcal{H} = \begin{pmatrix} -ic\partial_{z_1} & -g_p & 0 & 0 \\ -g_p & -i\gamma & -\Omega & 0 \\ 0 & -\Omega & \delta & g'_+ \\ 0 & 0 & g'_+ & -iv\partial_{z_1} \end{pmatrix} \otimes \begin{pmatrix} 1 & 0 & 0 & 0 \\ 0 & 1 & 0 & 0 \\ 0 & 0 & 1 & 0 \\ 0 & 0 & 0 & 1 \end{pmatrix} + \begin{pmatrix} 1 & 0 & 0 & 0 \\ 0 & 1 & 0 & 0 \\ 0 & 0 & 1 & 0 \\ 0 & 0 & 0 & 1 \end{pmatrix} \otimes \begin{pmatrix} ic\partial_{z_2} & -g_p & 0 & 0 \\ -g_p & -i\gamma & -\Omega & 0 \\ 0 & -\Omega & \delta & g'_- \\ 0 & 0 & g'_- & iv\partial_{z_2} \end{pmatrix} + V(z_1 - z_2) \Sigma^\dagger \Sigma, \quad (\text{B38})$$

with $\Sigma = (0, 0, 0, 0, 0, 0, 0, 0, 0, 0, 1, 0, 0, 0, 0, 0)$. All numerical results presented in the main text are based on solving this 16×16 partial differential equation set with a Gaussian initial pulse.

Appendix C: Comparison between spatial and temporal modulations of the coupling constant

In this section, we clarify several differences between spatial [$g(z) = g$ for $-L/2 < z < L/2$] and tempo-

ral [$g(t) = g$ for $-T/2 < t < T/2$] modulations of the

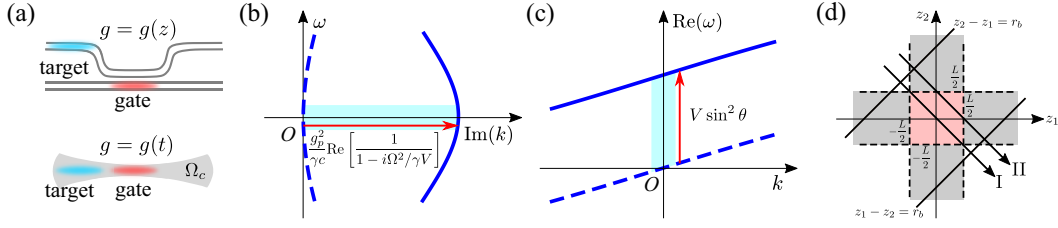


FIG. 6. (a) Illustration of spatial and temporal modulations of the coupling. (b) Illustration of the interaction induced momentum-mismatch coupling. (c) Illustration of the interaction induced energy-nonresonance coupling. (d) Illustration of the coupling region in the spatial modulation case.

coupling. Spatial modulation is straightforwardly implemented in the photonic coupling scheme [see the upper panel of Fig. 6(a)], while temporal modulation can be achieved by varying the intensity of the control field in the atomic coupling scheme [see the lower panel of Fig. 6(a)]. The temporal modulation of g can also be realized in the photonic coupling scheme by adopting photonic transition approach [42] or photonic Raman process [43], with the coupling controlled by refraction index modulation.

In fact, for spatial modulation of the coupling constant, the momentum (wave-vector) of the photon is not conserved, while the energy (frequency) of the photon remains conserved. The situation is reversed for temporal modulation. Thus, for spatial modulation, the coupling blockade originates from interaction induced large momentum mismatch [see Fig. 6(b)], i.e., $|g_p^2/\gamma c(1 - i\Omega^2/\gamma V)| \gg g/v$. In this case, perfect blockade requires the compressed length of the stored gate excitation to be smaller than the EIT blockade radius z_b and the coupling region $L < 2z_b$. For temporal modulation, coupling blockade occurs if the interaction induced energy shift $V \sin^2 \theta$ (in the frequency dimension) is much larger than the coupling g [see Fig. 6(c)], and perfect blockade requires $\sigma + \frac{1}{2}vT < r_b$ with σ the same compressed length of the target and gate photon.

Spatial modulation assisted coupling blockade can also be used for single-photon switching, but is not suitable for applications including entanglement generation or quantum beam splitting unless $\sigma \ll L$. This is due to the nonlocal property of the photon. Taking two counter propagating photons as an example, for the coupling region of length L [as shown in Fig. 6(d)], the separable two-photon wavefunction is coupled with entangled wavefunction only when $\{(-L/2 < z_1 < L/2) | (-L/2 < z_2 < L/2)\}$ (the pink region). For the wavefunction along path I, the initial separable two-photon wavefunction can be efficiently transformed to entangled state, while the wavefunction along path II propagates in regions where only one photon feels the nonzero couplings (gray region) for most of the time and thus entanglement cannot be efficiently generated.

Appendix D: Experimental considerations

In this section, we discuss necessary conditions for the experimental observation of our proposed scheme, mainly concerning by the trade-off between ideal blockade and linear EIT loss.

For DSPs with compressed pulse length σ and group velocity v_g , the bandwidth of the signal is $\Delta\omega \approx v_g/\sigma$. The loss caused by finite EIT transparency window contains two parts: the loss during the conversion between free space photon and DSPs over the length scale σ ; and the loss during the operation time g^{-1} over the length scale v_g/g , which are respectively given by

$$\xi = (\Delta\omega)^2 \frac{\gamma g_p^2}{c\Omega^4} \times \sigma, \quad \eta = (\Delta\omega)^2 \frac{\gamma g_p^2}{c\Omega^4} \times \frac{v_g}{g}. \quad (\text{D1})$$

The above equation together with the introduction of coupling blockade radius r_b defined by $C_6/r_b^2 = 2g$ and EIT blockade radius z_b defined by $C_6/z_b^2 = \Omega^2/\gamma$ yield $\sigma = \gamma c/(g_p^2 \xi)$ and $r_b = (\eta/2\xi^2)^{1/6} z_b$, which gives

$$r_b/\sigma = (\xi)^{2/3} (\eta/2)^{1/6} \times d_b, \quad (\text{D2})$$

where $d_b = g_p^2/(\gamma c) z_b$ characterizes the usual blockade optical depth [17].

As mentioned in the main text, ideal coupling blockade requires $r_b > \sigma$. Thus, for a fixed blockade optical depth d_b , Eq. (D2) indicates that there is a trade-off between the ratio r_b/σ and the linear EIT loss $\xi + \eta$, i.e., less loss would lead to worse blockade. In fact, a large optical depth d_b can reduce the loss to acceptable values while keeping the coupling blockade nearly perfect, e.g., for $\xi = 5\%$ and $\eta = 3\%$, $d_b = 15$ can ensure $r_b > \sigma$.

Restricting η to be 2.5%, we plot the operation fidelity \mathcal{F}_s of the produced entangled state (see Sec. IV B) versus the linear EIT loss ξ for different blockade optical depth. As shown in Fig. 7(a), the increase of the linear EIT loss results in a better operation fidelity (the fidelity during the operation process, not the total fidelity), and a higher d_b yields a higher \mathcal{F}_s for a fixed linear EIT loss. Thus, to achieve a high total fidelity, a higher blockade optical depth is preferred. The increase of blockade optical depth d_b can be achieved by using higher-lying Rydberg states, increasing the atomic density, and reducing the transverse area of the photonic mode. In the main text, we

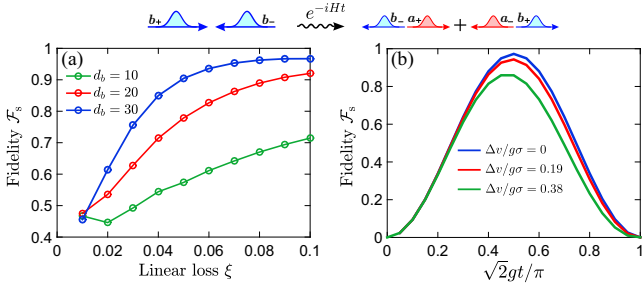


FIG. 7. (a) Fidelity of the generated symmetric entangled state versus linear EIT loss for the indicated value of blockade optical depth. (b) Oscillation of the fidelity \mathcal{F}_s for different group velocity mismatches.

use a large coupling constant $g_p = 20$ GHz, corresponding to $d_b = 38.46$. Such a strong atom-photon coupling can be achieved by using a Bose-Einstein condensate with an atomic density $\mathcal{N} \sim 10^{14} \text{cm}^{-3}$.

Another requirement arises from the finite life time τ_r of the Rydberg state. To ensure nearly lossless Rydberg excitation, the time duration for propagation inside the atomic ensemble should be much smaller than τ_r , i.e., $t \sim \sigma/v_g + 1/g = (1/\xi + \eta/\xi^2)\gamma/\Omega^2 \ll \tau_r$. For $\gamma/2\pi = 3$ MHz and $\Omega/2\pi = 5$ MHz used in the main text, $\xi = 5\%$ and $\eta = 3\%$ gives $t \approx 0.6 \mu\text{s}$, which meets the requirement as it is shorter than the typical life time τ_r of the Rydberg polariton (usually up to several microseconds [10]).

We also consider the influence of the group velocity mismatch on the blockade effect. The group velocity mismatch between the dark state polariton $\hat{\Psi}_{a\pm}(z)$ [group velocity being $v_g = c\Omega^2/(g_p^2 + \Omega^2)$] and linear light polariton $\hat{\Psi}_{b\pm}(z)$ (group velocity being v) is defined as

$\Delta v = v - v_g$. Intuitively, the influence of the group velocity mismatch is determined by the quantity $\Delta vt/\sigma$, i.e., a larger $\Delta vt/\sigma$ suggests a larger separation of the photonic wavefunction in different modes. We plot \mathcal{F}_s for different values of v [other parameters are the same as in Fig. 2(c) in the main text] in Fig. 7(b). If $\Delta v/g\sigma \ll 1$ is satisfied, the oscillation visibility remains high during the operation time $t \sim 1/g$.

For the single-photon switching in the photonic coupling scheme (spatial modulation case), we only need the stored gate photon to be compressed ($\sigma < z_b$), and the bandwidth of the target photon can be chosen well within the EIT transparency window. In this case, choosing $L = 2z_b$ and $gL/v = \pi/2$, the switching fidelity is approximately given by $\mathcal{F}_{\text{switch}} \approx \exp(-2g^2\gamma c/g_p^2 v^2 L) = \exp(-\pi^2/4d_b) \approx 1 - \pi^2/4d_b$. Such a quantum switching fidelity has the same scaling on d_b as in the novel polariton switching scheme recently proposed [27]. Although the fidelity of our scheme is slightly smaller than [27] in the small d_b region, our scheme possesses a larger bandwidth in the large d_b region, as the bandwidth of the target photon is not reduced by the strong interaction in the coupling blockade scheme.

For the atomic coupling scheme, we provide here a possible choice of level structures for ^{87}Rb atoms. In the scheme, one can choose $|e_+\rangle = |5P_{3/2}, F=2, m_F=1\rangle$, $|e_-\rangle = |5P_{3/2}, F=2, m_F=-1\rangle$, $|g\rangle = |5S_{1/2}, F=1, m_F=0\rangle$, $|d\rangle = |5S_{1/2}, F=2, m_F=0\rangle$, and $|r\rangle = |nS_{1/2}, J=1/2, m_J=-1/2\rangle$. The coupling Ω_c between $|d\rangle$ and $|r\rangle$ can be constructed using a two-photon process with an intermediate state $|5P_{1/2}, F=1, m_F=-1\rangle$. The z -direction wave-vectors k_1 , k_2 , and k_c of the control field Ω_1 , Ω_2 , and Ω_c should be tuned to satisfy the phase-matching condition $k_1 + k_2 - k_c = k_{\odot} - k_{\ominus}$.

-
- [1] D. E. Chang, V. Vuletić, and M. D. Lukin, *Nat. Photon.* **8**, 685 (2014).
- [2] C. Murray and T. Pohl, *Advances In Atomic, Molecular, and Optical Physics* **65**, 321 (2016).
- [3] O. Firstenberg, C. S. Adams, and S. Hofferberth, *J. Phys. B* **49**, 152003 (2016).
- [4] I. Friedler, D. Petrosyan, M. Fleischhauer, and G. Kurizki, *Phys. Rev. A* **72**, 043803 (2005).
- [5] H. Kimble, *Nature* **453**, 1023 (2008).
- [6] J. L. O'Brien, A. Furusawa, and J. Vučković, *Nat. Photon.* **3**, 687 (2009).
- [7] D. Chang, V. Gritsev, G. Morigi, V. Vuletic, M. Lukin, and E. Demler, *Nat. Phys.* **4**, 884 (2008).
- [8] J. Otterbach, M. Moos, D. Muth, and M. Fleischhauer, *Phys. Rev. Lett.* **111**, 113001 (2013).
- [9] M. Gullans, J. Thompson, Y. Wang, Q.-Y. Liang, V. Vuletić, M. D. Lukin, and A. V. Gorshkov, *Phys. Rev. Lett.* **117**, 113601 (2016).
- [10] C. R. Murray, I. Mirgorodskiy, C. Tresp, C. Braun, A. Paris-Mandoki, A. V. Gorshkov, S. Hofferberth, and T. Pohl, *Phys. Rev. Lett.* **120**, 113601 (2018).
- [11] K. M. Birnbaum, A. Boca, R. Miller, A. D. Boozer, T. E. Northup, and H. J. Kimble, *Nature* **436**, 87 (2005).
- [12] J. D. Thompson, T. Tiecke, N. P. de Leon, J. Feist, A. Akimov, M. Gullans, A. S. Zibrov, V. Vuletić, and M. D. Lukin, *Science* **340**, 1202 (2013).
- [13] A. Goban, C.-L. Hung, S.-P. Yu, J. Hood, J. Muniz, J. Lee, M. Martin, A. McClung, K. Choi, D. E. Chang, *et al.*, *Nat. Commun.* **5** (2014).
- [14] A. Reiserer and G. Rempe, *Rev. Mod. Phys.* **87**, 1379 (2015).
- [15] J. S. Douglas, T. Caneva, and D. E. Chang, *Phys. Rev. X* **6**, 031017 (2016).
- [16] E. Shahmoon, P. Grišins, H. P. Stimming, I. Mazets, and G. Kurizki, *Optica* **3**, 725 (2016).
- [17] A. V. Gorshkov, J. Otterbach, M. Fleischhauer, T. Pohl, and M. D. Lukin, *Phys. Rev. Lett.* **107**, 133602 (2011).
- [18] M. F. Maghrebi, M. J. Gullans, P. Bienias, S. Choi, I. Martin, O. Firstenberg, M. D. Lukin, H. Büchler, and A. V. Gorshkov, *Phys. Rev. Lett.* **115**, 123601 (2015).
- [19] T. Peyronel, O. Firstenberg, Q.-Y. Liang, S. Hofferberth, A. V. Gorshkov, T. Pohl, M. D. Lukin, and V. Vuletic, *Nature* **487**, 57 (2012).

- [20] O. Firstenberg, T. Peyronel, Q.-Y. Liang, A. V. Gorshkov, M. D. Lukin, and V. Vuletić, *Nature* **502**, 71 (2013).
- [21] S. Baur, D. Tiarks, G. Rempe, and S. Dürr, *Phys. Rev. Lett.* **112**, 073901 (2014).
- [22] H. Gorniaczyk, C. Tresp, J. Schmidt, H. Fedder, and S. Hofferberth, *Phys. Rev. Lett.* **113**, 053601 (2014).
- [23] C. Tresp, C. Zimmer, I. Mirgorodskiy, H. Gorniaczyk, A. Paris-Mandoki, and S. Hofferberth, *Phys. Rev. Lett.* **117**, 223001 (2016).
- [24] E. Distante, A. Padrón-Brito, M. Cristiani, D. Paredes-Barato, and H. de Riedmatten, *Phys. Rev. Lett.* **117**, 113001 (2016).
- [25] A. V. Gorshkov, R. Nath, and T. Pohl, *Phys. Rev. Lett.* **110**, 153601 (2013).
- [26] C. R. Murray, A. V. Gorshkov, and T. Pohl, *New J. Phys.* **18**, 092001 (2016).
- [27] C. R. Murray and T. Pohl, *Phys. Rev. X* **7**, 031007 (2017).
- [28] A. Yariv and P. Yeh, *Photonics: optical electronics in modern communications*, Vol. 6 (Oxford University Press New York, 2007).
- [29] M. Lukin, M. Fleischhauer, R. Cote, L. Duan, D. Jaksch, J. Cirac, and P. Zoller, *Phys. Rev. Lett.* **87**, 037901 (2001).
- [30] E. Urban, T. Johnson, T. Henage, L. Isenhower, D. Yavuz, T. Walker, and M. Saffman, *Nat. Phys.* **5**, 110 (2009).
- [31] A. Gaetan, Y. Miroshnychenko, T. Wilk, A. Chotia, M. Viteau, D. Comparat, P. Pillet, A. Browaeys, and P. Grangier, *Nat. Phys.* **5**, 115 (2009).
- [32] M. Fleischhauer and M. D. Lukin, *Phys. Rev. Lett.* **84**, 5094 (2000).
- [33] C. A. Christensen, S. Will, M. Saba, G.-B. Jo, Y.-I. Shin, W. Ketterle, and D. Pritchard, *Phys. Rev. A* **78**, 033429 (2008).
- [34] M. Bajcsy, S. Hofferberth, V. Balic, T. Peyronel, M. Hafezi, A. S. Zibrov, V. Vuletic, and M. D. Lukin, *Phys. Rev. Lett.* **102**, 203902 (2009).
- [35] E. Vetsch, D. Reitz, G. Sagué, R. Schmidt, S. Dawkins, and A. Rauschenbeutel, *Phys. Rev. Lett.* **104**, 203603 (2010).
- [36] E. Shahmoon, G. Kurizki, M. Fleischhauer, and D. Petrosyan, *Phys. Rev. A* **83**, 033806 (2011).
- [37] M. Langbecker, M. Noaman, N. Kjærgaard, F. Benabid, and P. Windpassinger, *Phys. Rev. A* **96**, 041402 (2017).
- [38] B. He, A. Sharypov, J. Sheng, C. Simon, and M. Xiao, *Phys. Rev. Lett.* **112**, 133606 (2014).
- [39] J. Johnson and S. Rolston, *Phys. Rev. A* **82**, 033412 (2010).
- [40] Y.-Y. Jau, A. Hankin, T. Keating, I. Deutsch, and G. Biedermann, *Nat. Phys.* **12** (2015).
- [41] L. Li and A. Kuzmich, *Nat. Commun.* **7**, 13618 (2016).
- [42] Z. Yu and S. Fan, *Nat. Photon.* **3**, 91 (2009).
- [43] M. Mrejen, H. Suchowski, T. Hatakeyama, C. Wu, L. Feng, K. O'Brien, Y. Wang, and X. Zhang, *Nat. Commun.* **6** (2015).